Involvement of Pazopanib and Sunitinib Aldehyde Reactive Metabolites in Toxicity and Drug–Drug Interactions in Vitro and in Patient Samples

Marie-Noelle Paludetto, Jean-Luc Stigliani, Anne Robert, Vania Bernardes-Génisson, Etienne Chatelut, Florent Puisset, Cécile Arellano

Involvement of pazopanib and sunitinib aldehyde reactive metabolites in toxicity and drug-drug interactions *in vitro* and in patient samples

Marie-Noëlle Paludetto,[†,‡,§] *Jean-Luc Stigliani,*[‡,||] *Anne Robert,*[||] *Vania Bernardes-Génisson,*[‡,||] *Etienne Chatelut,*[†,‡,§] *Florent Puisset,*[†,‡,§] *Cécile Arellano.*[†,‡,*]

[†]Centre de Recherches en Cancérologie de Toulouse (CRCT), INSERM UMR1037, Université de Toulouse, 2 avenue Hubert Curien, CS53717, 31037 Toulouse Cedex 1, France.

[‡]Université Paul Sabatier, Toulouse, France.

[§] Institut Claudius-Regaud, IUCT-O, Toulouse, France.

[||]Laboratoire de Chimie de Coordination du CNRS (LCC-CNRS), Université de Toulouse, 205 route de Narbonne, BP 44099, 31077 Toulouse, Cedex 4, France.

[*] Corresponding author: cecile.arellano@univ-tlse3.fr

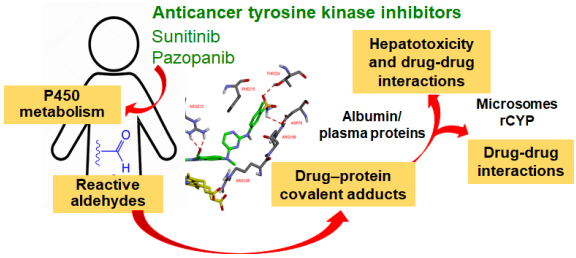

Toc Graphical abstract

ABSTRACT:

Tyrosine kinase inhibitors (TKI) are targeted anticancer drugs that have been successfully developed over the past two decades. To date, many of them (around 70%) require warnings for liver injury and five of them, including pazopanib and sunitinib, have Black Box Warning (BBW) labels. Although TKI-induced hepatotoxicity is the first cause of drug failures in clinical trials, BBW labels and market withdrawals, the underlying mechanisms remain unclear. However, the recent discovery of new reactive metabolites (RM) with aldehyde structures during pazopanib and sunitinib metabolism offers new perspectives for investigating their involvement in the toxicity of these two TKI. These hard electrophiles have a high reactivity potential toward proteins and are thought to be responsible for cytochrome P450 inactivation, drug-drug interactions (DDI) and liver toxicity. We report here, for the first time, the presence of these aldehyde RM in human plasma samples obtained during

drug monitoring. Docking experiments in the CYP3A4 active site were performed and showed that pazopanib and sunitinib fitting in the catalytic site are in accordance with their regioselective oxidation to aldehydes. They also suggested that aldehyde RM may react with lysine and arginine residues. Based on these results, we studied the reactivity of the aldehyde RM toward lysine and arginine residues as potential targets on the protein framework to better understand how these RM could be involved in liver toxicity and drug-drug interactions. Adduct formation with different hepatic and plasma proteins was investigated by LC-MS/MS and adducts between pazopanib or sunitinib aldehyde derivatives and lysine residues on both CYP3A4 and plasma proteins were indeed shown for the first time.

Key words: pazopanib, sunitinib, reactive aldehyde metabolites, lysine adduct, hepatotoxicity, drug-drug interactions.

1. INTRODUCTION

Tyrosine kinase inhibitors (TKI) are small molecular weight anticancer drugs targeting membrane-bound (receptors) and cytoplasmic tyrosine kinases that have emerged as important targets in oncology, due to their key role in cellular signaling and their frequent dysregulation in various cancers. Over the past two decades, many compounds have been successfully developed since the first-in-class drug, imatinib, was approved in 2001[1]. However, several

63 studies have shown that TKI, including pazopanib and sunitinib, which are oral
64 drugs prescribed over a long period of time to patients with co-medications
65 and are also P450 inhibitors, can cause Drug-Drug Interactions (DDI)[2–5]. To
66 date, among the 33 FDA-approved TKI, 22 (67%) require warnings for liver
67 injury in drug labelling with Black Box Warning (BBW) labels for five
68 compounds (lapatinib, pazopanib, ponatinib, sunitinib, and regorafenib)[6,7].
69 TKI-induced hepatotoxicity is a major clinical and industrial concern, since
70 drug-induced liver injury is the first cause of drug failures in clinical trials, BBW
71 labels and market withdrawals. Shah *et al.* indeed reported that 25–35% of
72 clinical trial patients treated with TKI showed a low-grade elevation in alanine
73 and/or aspartate aminotransferases, and approximately 2% of them
74 developed high-grade increases in serum transaminases, with a wide variability
75 among TKI[8].
76 Although little is known about the underlying mechanisms, it is thought that
77 liver toxicity could be due to reactive metabolites (RM) and as well as being
78 immune-related. RM reactivity is associated with the presence of electrophilic
79 moieties or radicals originating from the metabolic transformation, often
80 called bio-activation, of particular functional groups known as structural alerts
81 or toxicophores. RMs are able to covalently bind to proteins and DNA, causing
82 irreversible cellular damage and even cell death as well as DDI through P450
83 inactivation[9–12]. These so-called P450 time-dependent inhibitions (TDI) or
84 mechanism-based inhibitions (MBI) are characterized *in vitro* by a

85 concentration-, NADPH-, and time-dependence and involve RM arisen from
86 parent drug through a previous metabolic enzymatic step[13].
87 Drug bio-activation to RM that have the propensity to permanently inactivate
88 the enzyme involved in their generation could lead to enzyme MBI through
89 various and thoroughly reviewed[14–17] mechanisms, depending on RM structure
90 and reactivity. In any case, MBI is irreversible *in vivo*, so that the loss of
91 catalytic activity can only be restored by *de novo* synthesis of the enzyme,
92 resulting in modifications of drug metabolism (auto-inhibition) and
93 pharmacokinetic DDI (under or overdosing of co-administered drugs).
94 The formation of different RM has been suggested for several TKI[7]. While RM
95 formation has been proposed as a causative factor of liver toxicity[9,18], very
96 few published data actually support the role of RM in TKI-induced
97 hepatotoxicity. Until now, studies have mainly focused on the toxic role of *p*-
98 quinone-imines, for example for lapatinib in HepaRG cells[19–21] and for famitinib
99 in human primary hepatocytes[22]. Using HepG2 cells, Petrucci *et al.* suggested
100 that RM rather than the parent drug were involved in pazopanib liver toxicity[23].
101 Sunitinib oxidative defluorination involving P450 enzymes to generate a
102 reactive, potentially toxic quinone-imine was also reported more recently[18].
103 We have recently demonstrated the aldehyde RM formation during pazopanib
104 and sunitinib metabolic activation using P450 biomimetic models and human
105 liver microsomes (HLM)[24] (Figure 1). Pazopanib aldehyde derivatives have also
106 been reported in HLM incubations using a metabolomic approach[25]. Aldehyde

formation has otherwise been previously reported for several other TKI[26,27]. Although their involvement in DDI and toxicity was not further investigated, aldehydes are hard electrophiles with a high reactivity potential toward proteins and are thought to be responsible for P450 inactivation and toxicity[28,29]. Wang *et al.* indeed suggested a relationship between aldehyde formation and elevation of transaminases in pazopanib-treated mice[25].

Thus, studies are needed to investigate the molecular relationship between aldehyde RM and P450 inactivation and hepatotoxicity for pazopanib and sunitinib. Few studies have been carried out for this purpose in patient samples. We report here, for the first time, evidence of the formation of these drug-derived aldehydes in treated patients.

Sunitinib and pazopanib are mainly metabolized by CYP3A4 and to a lesser extent by CYP2C8 leading to metabolites that cause CYP3A4 TDI but do not affect CYP2C8 activity *in vitro*[3–5,30]. A docking study was performed in CYP3A4 catalytic site to gain more insight on the interactions of aldehyde metabolites with the protein framework in order to anticipate their putative involvement in liver toxicity, P450 inhibition and DDI. This study suggested that arginine and lysine residues, located in the catalytic site and the solvent channel of CYP3A4, close to the carbonyl aldehyde groups, could be potential targets to react with aldehyde RM. The reactivity of the aldehyde RM toward arginine and lysine residues of different hepatic (HLM, recombinant P450) and plasma (albumin) proteins was thus investigated by LC-MS/MS.

Figure 1

2. EXPERIMENTAL SECTION

2.1. Patients

Plasma samples were obtained from patients enrolled in the “SUP-R” trial (Institut Claudius Regaud, Toulouse, France, EUDRACT 2015-001051-68, NCT02555748). All patients gave written informed consent, and the study was approved by the Ethics Committee of the Midi-Pyrénées Region (Comité de Protection des Personnes Sud-Ouest et Outre-Mer III). It was an open-label, multicenter, non-randomized, phase IV clinical trial to examine the feasibility of sunitinib and pazopanib dose individualization based on therapeutic drug monitoring. Patients were treated with 800 mg of pazopanib once daily or with 50 mg of sunitinib once daily for four weeks, followed by a washout period of two weeks. Blood samples were obtained at day 1 and day 15 of cycle 1 and cycle 2. Each blood sample (4 mL in a EDTA tube) was then processed by centrifugation for 10 minutes at 1500g. Plasma supernatant was stored in cryotubes at -20°C until subsequent analysis.

2.2. Docking experiments: computational procedure

The crystallographic structures of CYP3A4 were taken from the Brookhaven Protein Data Bank. A large number of 3D structures of CYP3A4 are available. We chose two, making a compromise between the resolution of the structures and the number of missing residues, preferably the lowest possible. The first structure (PDB entry 6BCZ) is complexed with a ritonavir-like inhibitor and has a resolution of 2.23 Å[31]. The second (PDB entry 1TQN) is an apo form and has a resolution of 2.05 Å[32].

The ligands and water molecules were extracted from the PDB files. MolProbity software was used to assign the position of hydrogen atoms and the protonation state of histidines[33]. Hydrogen atoms were independently added onto the crystal structure of the heme prosthetic group. The ligands of this study, pazopanib and sunitinib aldehydes, were thoroughly built and fully optimized before the docking stage with the PM7 Hamiltonian implemented in the MOPAC2016 quantum chemistry package (MOPAC2016, James J. P. Stewart, Stewart Computational Chemistry, Colorado Springs, CO, USA, HTTP://OpenMOPAC.net (2016))[34]. The docking calculations were performed with the docking program Autodock Vina v1.1[35]. The Autodock graphical interface AutoDockTools was used to keep polar hydrogens and add partial charges to the proteins using the Kollman United charges[36]. The search space was included in a box of 24 × 24 × 24 Å, centered on the binding site of the ligands and heme. The side chain of the S119, R212, I301, F304 and E374 residues that are exposed on the surface of the catalytic cavity were allowed

Code de champ modifié

172 to rotate during the docking procedures. Flexible torsions of side chains and
173 ligands were assigned with Autotors, an auxiliary module of AutoDockTools.
174 For each calculation, 15 poses ranked according to the scoring-function of
175 Autodock Vina were obtained.
176
177 **2.3. Materials and instruments**
178 Sunitinib L-malate and pazopanib hydrochloride were purchased from
179 Alsachim (Illkirch-Graffenstaden, France). All solvents and commercially
180 available reagents were used without further purification. Acetonitrile and
181 methanol were provided by Scharlau (Barcelona, Spain), and formic acid by
182 Merck (Darmstadt, Germany). Ammonium formate, ammonium
183 hydrogencarbonate, sodium acetate, sodium cyanoborohydride, sodium
184 dihydrogenphosphate, disodium hydrogenphosphate, D,L-dithiothreitol,
185 dimethylsulfoxide (DMSO), human serum albumin, pronase, chymotrypsin,
186 trysin and L-arginine were purchased from Sigma-Aldrich (St Quentin-Fallavier,
187 France). L-Lysine•HCl came from Alfa Aesar (Ward Hill, USA) and calcium
188 chloride from Acros organics (Illkirch, France). Blank plasma from healthy
189 donors was provided by « Etablissement Français du Sang » (EFS, Toulouse,
190 France). Aldehyde metabolites **1a-CHO** and **2-CHO** for control or spiking
191 experiments were prepared through drug biomimetic oxidation using
192 manganese porphyrin complexes as catalysts, as previously reported[24].
193 Recombinant Human CYP3A4 (Ref. 456202), pooled human liver microsomes

194 (Ref. 452161), NADPH regenerating solutions (Ref. 451220, 451200) were
195 purchased from Corning (Woburn, USA).
196
197 *LC-MS analyses.* Identification of aldehyde metabolites **1a-CHO** and **2-CHO** in
198 human plasma were performed by UPLC-MS/MS with an UPLC Waters Acquity
199 system equipped with a Waters TQ-S micro mass spectrometer (triple
200 quadrupole detector), an electrospray ionization source (ESI) and MassLynx™
201 software. UPLC chromatographic separations were performed on an Acquity
202 UPLC® BEH Shield RP18 (1.7 μm, 2.1 x 50 mm) column (Waters, Milford, MA,
203 USA) at a flow rate of 0.3 mL/min and a column temperature of 30°C. Eluent
204 A was ammonium formate 5 mM pH = 3.2 and eluent B was formic acid 0.1%
205 (v/v) in acetonitrile. Eluting conditions were a linear gradient of A and B as
206 follows: the percentage of B, initially set at 2%, stayed at 2% until 0.5 min,
207 increased to reach 60% (t = 3.5 min), 100% (t = 4 min), stayed at 100%
208 until 4.5 min, then returned to initial conditions over 0.5 min. Afterward, the
209 system was re-equilibrated for 1 min before the following injection. The mass
210 spectrometer was operated in positive ionization mode (ESI^+), using cone
211 voltages of 60 or 80 V and collision energy of 30 eV. Mass spectra for L-
212 lysine adduct characterization were acquired in Full Scan mode (*m/z* range
213 50-650 amu for **1a-CHO** and **2-CHO**). Multiple Reaction Monitoring (MRM)
214 mode was used for **1a-CHO** and **2-CHO** detection in human plasma. MRM

transitions were as follows: for **1a-CHO**: *m/z* 452>343, 328; for **2-CHO**: *m/z* 413>340, 268.

Identification of lysine adducts of **1a-CHO** and **2-CHO** in protein samples (human plasma, human serum albumin, HLM, recombinant CYP3A4 (rCYP3A4)) was performed by UPLC-MS/MS with an RS 3000 UHPLC system (ThermoFisher Scientific) equipped with an AB Sciex QTRAP 4500 mass spectrometer (triple quadrupole detector), an electrospray ionization source (ESI) and Analyst™ software. UPLC chromatographic separations were performed with the same column and under the same eluting conditions, reported above. The mass spectrometer was operated in positive ionization mode (ESI^+), using cone voltages of 40 or 60 V and collision energies of 30 or 40 eV. MRM mode was used for lysine adduct detection in protein samples with the following MRM transitions: for **1a-CHO**–lysine adduct: *m/z* 582.2>436.2; for **2-CHO**–lysine adduct: *m/z* 543.2>326.1.

2.4. Preparation of lysine adduct standards

*Reaction of **1a-CHO** and **2-CHO** with L-lysine*: an aliquot of an aldehyde-containing medium (ca. 2 μmol of **1a-CHO** or **2-CHO** prepared as previously described[24] was dissolved in H_2O/CH_3OH (400 μL, 37/63 v/v). Sodium acetate (160 μmol) and L-lysine (80 μmol) were then added to afford imine derivatives.

Preparation of stable adducts: the one pot reductive amination of the imine derivatives was performed by $NaBH_3CN$ (three additions of 20 µL of a 1.3 M solution in methanol, *i.e.* ca. 40 eq. in regard to **1a-CHO** or **2-CHO**, every 30 minutes) over 120 minutes at 37°C. The crude reaction media were then analyzed by UPLC-MS.

2.5 Spiking experiments of 1a-CHO and 2-CHO in human protein samples.

Human plasma. An aliquot of an aldehyde-containing medium (ca. 20 nmol of **1a-CHO** or **2-CHO**, prepared as previously described[24], in 0.8 µL of DMSO) was added in human plasma (250 µL). During incubation at 37°C for 120 minutes, reductive amination was performed by $NaBH_3CN$ (four additions of 0.5 µL of a 1.25 M solution in methanol, *i.e.* ca. 125 eq. in regard to **1a-CHO** or **2-CHO**, every 30 minutes). The crude reaction media were then digested by proteases.

Human serum albumin. An aliquot of an aldehyde-containing medium (ca. 20 nmol of **1a-CHO** or **2-CHO**, prepared as previously described[24], in 0.8 µL of DMSO) was added to a mixture of human serum albumin (3 µL of a 40 g/L solution in 0.1 M phosphate buffer pH = 7.4) and 0.1 M phosphate buffer (pH = 7.4, final volume = 250 µL). During incubation at 37°C for 120 minutes, reductive amination was performed by $NaBH_3CN$ (four additions of 0.5 µL of a 1.25 M solution in methanol, *i.e.* ca. 125 eq. in regard to **1a-CHO** or **2-CHO**,

every 30 minutes). The crude reaction media were then digested by proteases.

Human liver microsomes/recombinant CYP3A4. An aliquot of an aldehyde-containing medium (ca. 20 nmol of **1a-CHO** or **2-CHO**, prepared as previously described[24], in 0.8 μL of DMSO) was added to a mixture of human liver microsomes (final protein concentration = 0.5 mg/mL) or recombinant CYP3A4 (final rCYP3A4 concentration = 20 pmol/mL) and 0.1 M phosphate buffer (pH = 7.4, final volume = 250 μL). During incubation at 37°C for 120 minutes, reductive amination was performed by $NaBH_3CN$ (four additions of 0.5 μL of a 1.25 M solution in methanol, *i.e.* ca. 125 eq. in regard to **1a-CHO** or **2-CHO**, every 30 minutes). The crude reaction media were then digested by proteases.

2.6. Human liver microsomes and recombinant CYP3A4 incubations.

Microsomal incubations were performed according to supplier protocol. An aliquot of human liver microsomes (final protein concentration = 2 mg/mL) was added to a mixture of NADPH regenerating solutions A (50 μL), B (10 μL) and 0.1 M phosphate buffer (pH = 7.4, final volume = 250 μL). After pre-incubation at 37°C for 5 minutes, microsomal incubations were started by the addition of pazopanib **1** or sunitinib **2** in DMSO solutions (final substrate concentration = 100 μM, final DMSO concentration = 0.2%). The mixture was then kept at 37°C for 30 minutes to ensure aldehyde formation. Reductive

amination was then performed by $NaBH_3CN$ (four additions of 0.5 μL of a 1.25 M solution in methanol, *i.e.* 100 eq. in regard to **1** or **2**, every 30 minutes, final methanol concentration = 0.8%) over 120 minutes at 37°C. The incubation media were then subjected to proteolytic digestion. The same protocol was followed with recombinant CYP3A4 (final rCYP3A4 concentration = 80 pmol/mL).

2.7. Protein digestion

Protein denaturation was achieved by heating the mixture to 60°C over 30 minutes. Disulfide bonds were reduced by addition of D, L-dithiothreitol (DTT, 50 μL of a 50 mM solution in 50 mM NH_4HCO_3 pH = 8). The mixture was then incubated at 60°C for one hour. Protein digestion was performed by the addition of trypsin, chymotrypsin, pronase E (100 μL of a 12.5 mg/mL solution of each protease in 50 mM NH_4HCO_3 pH = 8), acetonitrile (50 μL) and calcium chloride (100 μL of a 25 mM solution in water). The mixture was kept overnight at 37°C. Proteolytic digestion was stopped by the addition of 5 μL of formic acid 1% in water. The mixture was then centrifuged for 20 minutes at 4000 g at room temperature. The supernatants were then analyzed by UPLC-MS to characterize lysine or arginine adducts of sunitinib and pazopanib aldehyde metabolites. The following modifications to the above-described proteolytic digestion protocol were made for:

300 *i) HLM incubations in the presence of pazopanib **1***: after protein denaturation,
301 incubation media were centrifuged for 20 minutes at 4000 g at 40°C. The
302 protein pellets were then subjected to proteolytic digestion [DTT (20 µL of a
303 125 mM solution in 50 mM NH_4HCO_3 pH = 8), proteases (20 µL of a 62.5
304 mg/mL solution of each protease in 50 mM NH_4HCO_3 pH = 8) and calcium
305 chloride (10 µL of a 250 mM solution in water)];
306 *ii) HLM incubations in the presence of sunitinib **2***: after protein denaturation,
307 incubation media were centrifuged for 20 minutes at 4000 g at 40°C. The
308 protein pellets were then treated by DTT and incubated at 60°C for 1 hour
309 before proteolytic digestion;
310 *iii) rCYP3A4 incubations in the presence of pazopanib **1***: after proteolytic
311 digestion, supernatants of 10 incubations were pooled before UPLC-MS
312 analyses.
313
314 ## 3. RESULTS AND DISCUSSION
315 ### 3.1. Aldehyde identification in patient plasma samples
316 Aldehyde metabolites **1a-CHO** and **2-CHO** have been recently prepared *in vitro*
317 using chemical models[24] or HLM[24,25] (Figure 1). These aldehydes resulted from
318 the oxidation of the alcohol derivatives **1-CH_2OH** and **2-CH_2OH** previously
319 reported, respectively in human plasma for pazopanib **1**[37,38] and in rats,
320 monkeys and dogs for sunitinib **2**[39]. Wang *et al.* have also detected **1b-CHO**
321 in mice feces and urine[25], that we did not observe using biomimetic P450

models or HLM. Speed *et al*[40] reported the formation of a series of mono-oxygenated metabolites giving the same product ions (*m/z*: 415, fragments at *m/z*: 342, 299) and consistent with oxidation on sunitinib indolylidene/dimethylpyrrole moiety. Although the exact position of the oxidation could not be elucidated by LC-MS alone, such metabolites, detected in rat, monkey and human feces, are consistent with **2-CH_2OH**. In addition, Speed *et al* have reported unidentified metabolites, some of them cannot be ruled out as aldehydes.

The formation of aldehyde RM **1a-CHO** and **2-CHO** *in vivo* was investigated in plasma samples from patients treated, respectively, with pazopanib or sunitinib. Screening for **1a-CHO** and **2-CHO** was performed by UPLC-MS/MS at two characteristic MRM transitions for each compound to ensure specificity, in comparison with aldehyde standards prepared beforehand by biomimetic oxidations[24]. Despite reactivity of the aldehyde function, **1a-CHO** and **2-CHO** have been unambiguously detected in patient plasma samples during drug monitoring at 3.96 min (*m/z*: 452>343; 452>328) for pazopanib (Figure S-1B, C) and at 4.22 min (*m/z*: 413>268; 413>340) for sunitinib (Figure S-2B, C), consistently with the retention times of the corresponding standards (Figures S-1A and S-2A). Since no other peak was shown in the chromatograms (Figures S-1B, C and S-2B, C), **1b-CHO** was not detected in patient plasma samples. The exact quantification of these metabolites could not be carried out since the response factor of metabolites could not be

344 determined; but the time course relative evolution of the aldehyde contents
345 based on the related peak areas was established during drug monitoring at
346 different days of treatment cycles. Figure 2 illustrates the aldehyde profiles
347 over time (**1a-CHO**, *m/z* = 452>343 and **2-CHO**, *m/z* = 413>340) that
348 paralleled those of the parent drugs, both for pazopanib and sunitinib,
349 suggesting that the rate of aldehyde formation was lower than their rate of
350 elimination through bio-transformation, which is consistent with their
351 reactivity.
352 Moreover, monitoring at another MRM characteristic transition for each
353 aldehyde RM (**1a-CHO**, *m/z* = 452>328 and **2-CHO**, *m/z* = 413>340) gave
354 the same profiles, thus supporting the specificity of aldehyde detection.
355
356 **Figure 2**
357
358 The detection of drug-derived aldehydes in plasma of patients treated with
359 pazopanib or sunitinib is very important and provides evidence that the
360 reactive, potentially toxic metabolites are in fact generated *in vivo*. It also
361 confirms that metalloporphyrin-catalyzed biomimetic oxidations or HLM are
362 useful drug oxidation models[24] to provide relevant metabolites that can be
363 used as authentic standards and advance their study.
364
365 **3.2. Molecular docking of aldehyde metabolites**

366 Since molecular docking is a useful approach to predict molecular interactions,
367 docking experiments were performed to elucidate whether these electrophilic
368 aldehyde RM could be involved in CYP3A4 TDI and also in liver toxicity, through
369 covalent coupling with nucleophilic amino acid residues on P450 protein
370 framework. Aiming to identify putative amino acid targets that could interact
371 with the carbonyl aldehyde groups, **1a-CHO** and **2-CHO** were docked in
372 CYP3A4 catalytic site (PDB entries: 1TQN and 6BCZ). For both aldehyde RM,
373 binding modes were very close to those of parent molecules (see
374 supplementary data for docking of parent molecules Figures S-3, S-4). These
375 observations supports the regioselective oxidation of pazopanib ($-C_7$-CH3)
376 and sunitinib ($-C_{11}$-CH3) respectively to **1a-CHO** and **2-CHO** by CYP3A4.
377
378 ***Pazopanib aldehyde*** - Binding modes found with 1TQN and 6BCZ crystals were
379 quite similar for **1a-CHO.** In both structures, the first pose was oriented in the
380 same way so that the indazole ring was nearly coplanar with the heme center,
381 and the sulfonamide group made hydrogen bonds with Asp76 and Thr224
382 (1TQN, Figure 3A) and with Asp76 (6BCZ, Figure 3B). The predicted binding
383 free energies were -12.3 and -11.6 kcal/mol for 1TQN and 6BCZ, respectively.
384 It is noteworthy that the carbonyl aldehyde group of pazopanib RM was close
385 to the basic amino acid Arg212 (3.4 or 2 Å between the guanidino and the
386 carbonyl groups, Figure 3A, 3B respectively), thus suggesting a possible
387 reaction between **1a-CHO** and Arg212.

388

389 ***Sunitinib aldehyde*** - With 1TQN, **2-CHO** indolinone ring was inserted between
390 Phe215 and Arg106, and the terminal trialkylammonium group was located in
391 front of the heme. Furthermore, the interaction could be stabilized by
392 hydrogen bonds between the aldehyde function and Glu374 and Arg105
393 (Figure 3C). The predicted binding free energy was -10.1 kcal/mol. With the
394 6BCZ crystal, Autodock Vina provided two alternative poses with similar
395 energy, which were arranged head to tail with each other. In the first pose
396 (ΔG = -9.7 kcal/mol), the indolinone ring was stacked with the heme
397 macrocycle, and the trialkylammonium group was placed between the Arg106
398 and Phe215 residues (Figure 3D). The carboxaldehyde group formed
399 hydrogen bonds with the NH groups of Glu374 and Arg105 residues (Figure
400 3E). The second pose (ΔG = -9.6 kcal/mol) was, for its part, similar to the
401 conformation found with 1TQN and exhibited the same non-bonding
402 interactions, thus suggesting a possible reaction between **2-CHO** and these
403 amino acid residues.

404

405 **Figure 3**

406

407 Docking experiments showed that several arginine residues are located in
408 CYP3A4 active site, in close vicinity of **1a-CHO and 2-CHO** carboxaldehyde
409 groups (Figure 3). They also revealed the presence of a large number of

accessible lysine residues (37) on the protein surface, and more specifically in the solvent channel of CYP3A4 (Figure S-5). These results suggest that interactions between aldehyde RM and arginine residues (in the active site) or lysine residues (when metabolites leave the active site) could be expected and potentially be responsible for the formation of covalent protein-drug adducts and thereby for CYP3A4 TDI. In addition, covalent coupling of **1a-CHO** and **2-CHO** on CYP3A4 could also be involved in immune-related liver injury. RM coupling to P450 enzymes could indeed trigger an auto-immune response leading to hepatotoxicity as it has been previously reported for other drugs[41,42]. CYP3A4 therefore appears to be a potential target for aldehydes, this does not exclude the reaction of aldehydes with other proteins that can contribute to toxicity.

3.3. Proof of concept of protein-drug coupling

To support the hypothesis that reactions between pazopanib or sunitinib aldehydes and arginine or lysine residues may occur *in vivo*, we investigated the formation of arginine or lysine adducts in different hepatic (recombinant CYP3A4, HLM) and plasma (albumin) protein samples. Because of the presence of a free amino group on its side chain, lysine could be a good target for reactive electrophiles like aldehyde RM. Lysine adducts with different drugs have indeed been previously reported *in vitro*[43,44] and *in vivo*[45]. Reactions between aldehydes and amines affording imine derivatives are

known to be reversible in aqueous media. Thus, adduct formation was shown after reductive amination of imine derivatives by NaBH3CN *in vitro.*

To facilitate the identification of lysine and arginine adducts in protein samples, adduct formation was first investigated with lysine and arginine amino acids in preliminary experiments. The reaction between **1a-CHO** or **2-CHO** generated through biomimetic oxidations catalyzed by metalloporphyrins[24] and free lysine or arginine (40 mole eq.) yielded **1a-CHO** or **2-CHO** lysine adducts. As shown in Figure 4A, in the full scan chromatogram, lysine adduct of **1a-CHO** was detected at 3.20 min and was characterized by the presence of the $[M+H]^+$ ion (*m/z*: 582) and the MS/MS fragmentation pattern corresponding to the loss of lysine (*m/z*: 436) and lysine fragmentation (*m/z*: 130, 218). Fragmentation of the bond between N8 and the indazole ring provided ions at *m/z*: 291 and 190 with subsequent lysine fragmentation. These results showing the formation of covalent adducts between free lysine and **1a-CHO** confirmed the reactivity of this aldehyde RM toward the lysine ε-amino group. Similarly, lysine adduct of **2-CHO** was detected at 3.43 min and was characterized by the $[M+H]^+$ ion (*m/z*: 543) in the mass spectrum and by the MS/MS fragmentation pattern corresponding to the loss of lysine (*m/z*: 397), the loss of lysine and the diethylamine side chain (*m/z*: 326) or the diethylamine-ethylamine side chain (*m/z*: 283) (Figure 4B). MS/MS fragmentation pattern did not allow to exclude the coupling between **2-CHO** and the lysine α-amino group. However,

454 a small peak at *m/z* 469 (magnified in the frame) corresponding to the loss
455 of the α-amino acid moiety could be in favor of the coupling at the ε-amino
456 group. Thus, by analogy with **1a-CHO**, the structure of the adduct resulting
457 from the coupling of **2-CHO** at the lysine ε-amino group was shown in Figure
458 4B.
459 **Figure 4**
460
461 Based on these results (Figure 4), the characteristic MRM transitions at *m/z*:
462 582>436 for **1a-CHO** lysine adduct and at *m/z*: 543>326 for **2-CHO** lysine
463 adduct were selected in order to detect covalent adducts between these drug
464 aromatic aldehydes and several proteins (Figures 5 and 6, traces A).
465 Hepatic proteins are expected to be the primary targets of reactive aldehydes
466 since they are involved in forming the latter, thus making HLM and
467 recombinant P450 (rCYP) relevant models *in vitro*. Plasma proteins, including
468 albumin, have also been used as surrogate proteins since plasma samples are
469 easier to collect than liver tissues from patients in a clinical perspective[45–47].
470 In protein samples, proteolytic digestion was performed with a protease
471 cocktail (trysin, chymotrypsin and pronase) prior to LC-MS analyses to ensure
472 lysine adduct detection. These analyses were performed with a QTRAP LC-MS
473 apparatus for high sensitivity (this is why the retention times were slightly
474 different in comparison with Figure 4). The assignment of the chromatogram
475 peaks was done by spiking blank biological matrices (human plasma, human

476 albumin, HLM and rCYP3A4) with **1a-CHO** or **2-CHO** generated by biomimetic
477 oxidations catalyzed by metalloporphyrins as previously reported[24]. The
478 formation of lysine adducts of **1a-CHO** or **2-CHO** in plasma and albumin (3.03
479 min, *m/z*: 582>436, Figures 5B or 6B, respectively) and with HLM and
480 rCYP3A4 proteins (3.34 min, *m/z*: 543>326, Figures 5C or 6C, respectively)
481 was demonstrated by the presence of MRM peaks at the same retention time
482 as with free lysine (Figures 4 A and B). Lysine adducts were then detected in
483 HLM incubations and in incubation with rCYP3A4, supporting that **1a-CHO**
484 generated in HLM and rCYP3A4 incubations was able to readily react with
485 lysine residues on the P450 protein framework (Figure 5D). Similar results
486 were obtained for sunitinib biotransformation in HLM and rCYP3A4, since
487 lysine adducts of **2-CHO** were also detected in these conditions (Figure 6D).
488 **Figure 5**
489 **Figure 6**
490
491 Since docking experiments revealed that **1a-CHO** and **2-CHO** carbonyl
492 aldehyde groups are in close vicinity of arginine residues in CYP3A4 active
493 site, we also investigated the putative formation of arginine-aldehyde
494 adducts. Arginine guanidinium group can react with aldehydes to afford Schiff
495 bases, as has been shown with unsaturated aldehydes and formaldehyde[48–50].
496 Thus, the approach described above for lysine was also applied to examine if
497 arginine adducts in different protein samples could be formed. Although we

found low amounts of arginine adducts of **1a-CHO** and **2-CHO** after reaction with free arginine (data not shown), we did not detect any arginine adduct in protein samples after proteolytic digestion (data not shown). This could be explained by the lower nucleophilicity of the guanidinium group when compared to lysine primary amine in these biological conditions.

Until now, **1a-CHO** and **2-CHO** lysine adducts were not detected in patient plasma samples, probably due to their very low concentrations. However, this work advances the field by showing that aldehyde metabolites of pazopanib and sunitinib (**1a-CHO** and **2-CHO)** are found in patient samples and that these aldehyde RMs are able to react with proteins on lysine residues (shown *in vitro*).

Among other potential causative factors (mitochondrial toxicity, bile salt export pump and UDP-glucuronosyltransferase inhibition, genetic and immunologic polymorphisms[6,20,51–56], it could be hypothesized that the coupling of aldehydes with lysine residues of proteins (CYP3A4 and hepatic proteins) may be involved in hepatotoxicity. Lysine adduct formation could also explain CYP3A4 TDI and hence may contribute to pazopanib and sunitinib DDI.

Figures legend

Figure 1: Structures of pazopanib (**1**), sunitinib (**2**) and their related alcohol (**1-CH₂OH** and **2-CH₂OH**) and aldehyde metabolites (**1-CHO** and **2-CHO**).

Figure 2: Analyses of patient plasma samples during pazopanib or sunitinib treatment. 1) patients treated with pazopanib : detection of aldehyde **1a-CHO** (▲: *m/z* = 452>343) along with pazopanib (□) in the plasma samples of three patients (panels 1A, 1B, and 1C, respectively). 2) patients treated with sunitinib : detection of aldehyde **2-CHO** (■: *m/z* = 413>268) along with sunitinib (○) in the plasma samples of three patients (panels 2A, 2B, and 2C, respectively). D1C1: day 1, cycle 1; D15C1: day 15, cycle 1; D1C2: day 1, cycle 2; D15C2: day 15, cycle 2.

Figure 3: Molecular docking into the catalytic cavity of crystal structure of CYP3A4: A) **1a-CHO** / 1TQN; B) **1a-CHO** / 6BCZ; C) **2-CHO** / 1TQN, D) **2-CHO** / 6BCZ. The red dotted lines represent the non-bonding interactions (*i.e.* Hydrogen bonds, π-stacking or π-cation).

Figure 4: Lysine adducts A) with pazopanib aldehyde **1a-CHO**. LC-MS chromatograms in Full Scan mode, B), mass spectra. C) with sunitinib aldehyde **2-CHO**. LC-MS chromatograms in Full Scan mode, D) mass spectra, insert frame: magnified MS (*m/z*: from 450 to 500). Adduct structures in inserts.

Figure 5: LC-MS MRM chromatograms of lysine adducts of pazopanib aldehyde **1a-CHO** (RT = 3.0 min, m/z: 582 > 436). A) standard lysine adduct obtained through reaction of **1a-CHO** with free lysine; B) in plasma and albumin spiked with **1a-CHO** generated during biomimetic oxidations with metalloporphyrins; C) in HLM and rCYP3A4 spiked with **1a-CHO** generated

during biomimetic oxidations with metalloporphyrins; D) in HLM and rCYP3A4 incubations. B, C, D: adducts were detected after proteolytic digestion.

Figure 6: LC-MS MRM chromatograms of lysine adducts of sunitinib aldehyde **2-CHO** (RT = 3.3 min, *m/z*: 543.2>326.1). A) Standard lysine adduct obtained through reaction of **2-CHO** with free lysine; B) in plasma and albumin spiked with **2-CHO** generated during biomimetic oxidations with metalloporphyrins; C) in HLM and rCYP3A4 spiked with **2-CHO** generated during biomimetic oxidations with metalloporphyrins; D) in HLM incubations and rCYP3A4 incubations. B, C, D: adducts were detected after proteolytic digestion.

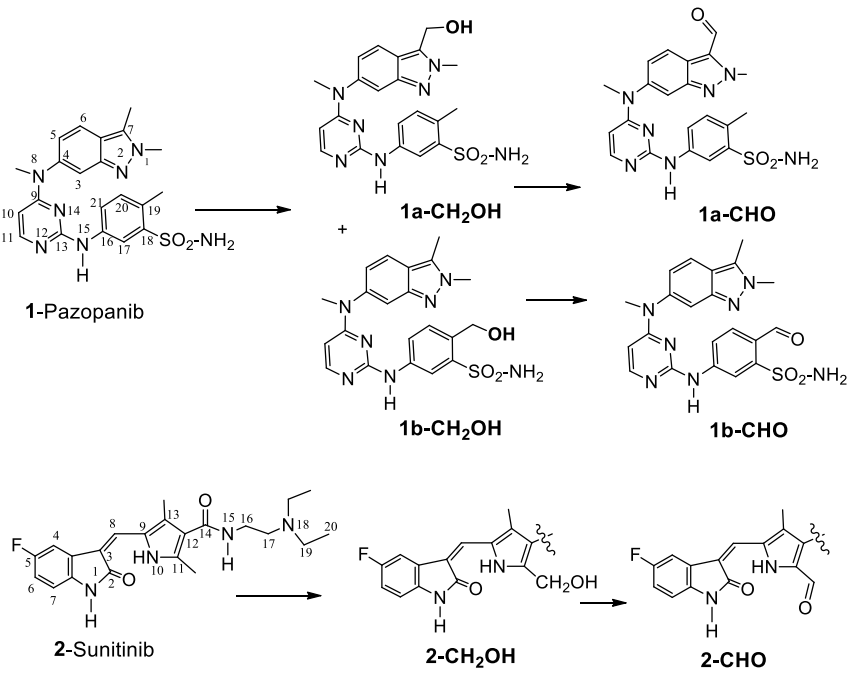
1-Pazopanib
1a-CH2OH
1a-CHO
1b-CH2OH
1b-CHO
2-Sunitinib
2-CH2OH
2-CHO

Figure 1

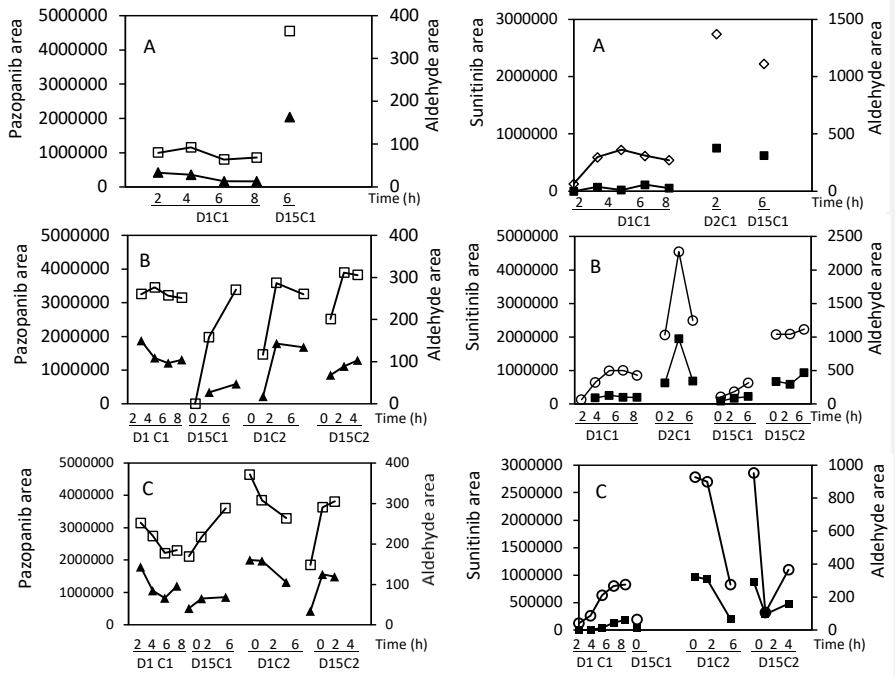
A
B
C
Pazopanib area
Sunitinib area
Aldehyde area
Time (h)
D1C1
D15C1
D2C1
D1 C1
D15C2
D1C2

Figure 2

552

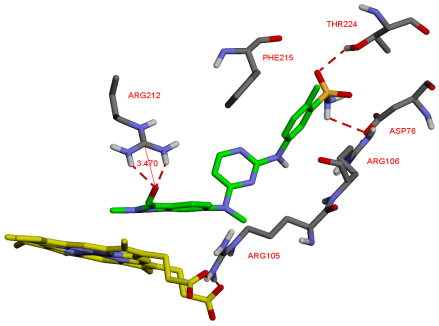

A) **1a-CHO** / 1TQN

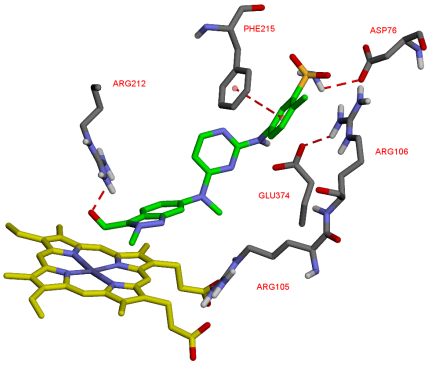

B)) **1a-CHO** / 6BCZ

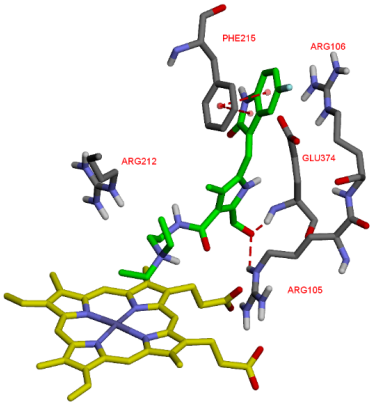

C) **2-CHO** / 1TQN

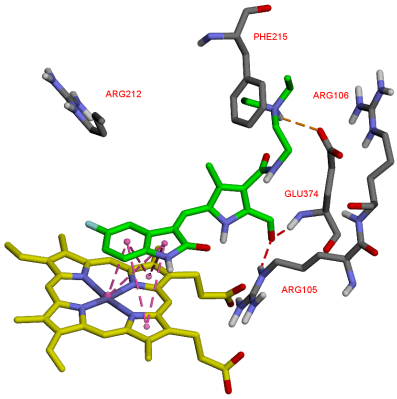

D) **2-CHO** / 6BCZ (Pose 1)

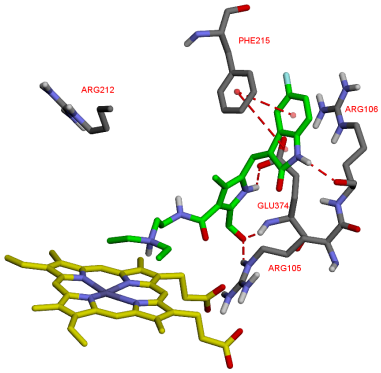

E) **2-CHO** / 6BCZ (Pose 2)

Figure 3

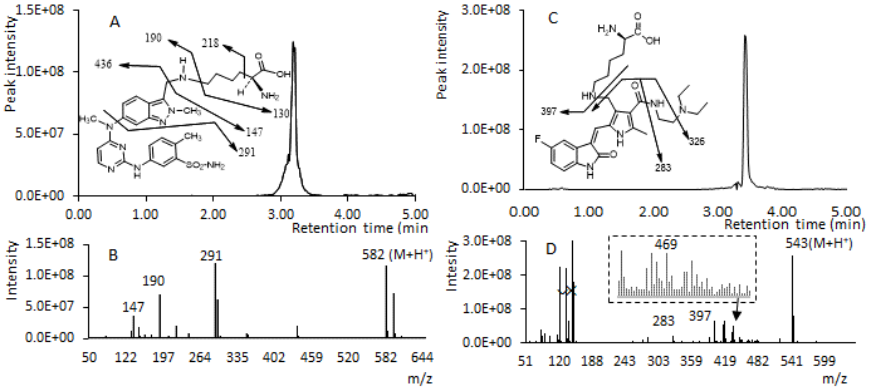
A
Peak intensity
1.5E+08
1.0E+08
5.0E+07
0.0E+00
0.00
1.00
2.00
3.00
4.00
5.00
Retention time (min
190
218
436
130
147
291
B
Intensity
582 (M+H+)
C
3.0E+08
2.0E+08
397
326
283
D
469
543(M+H+)
m/z

Figure 4

553

554

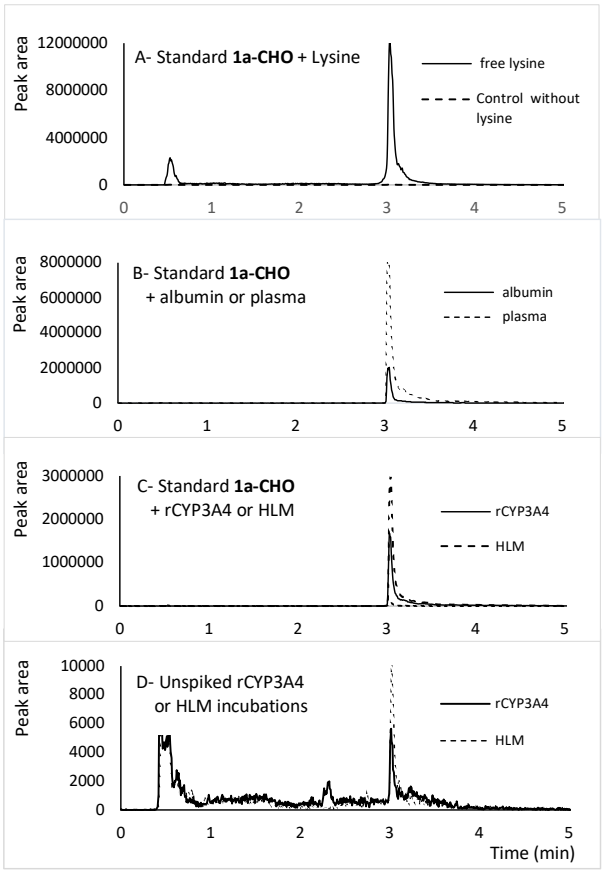

Figure 5

555

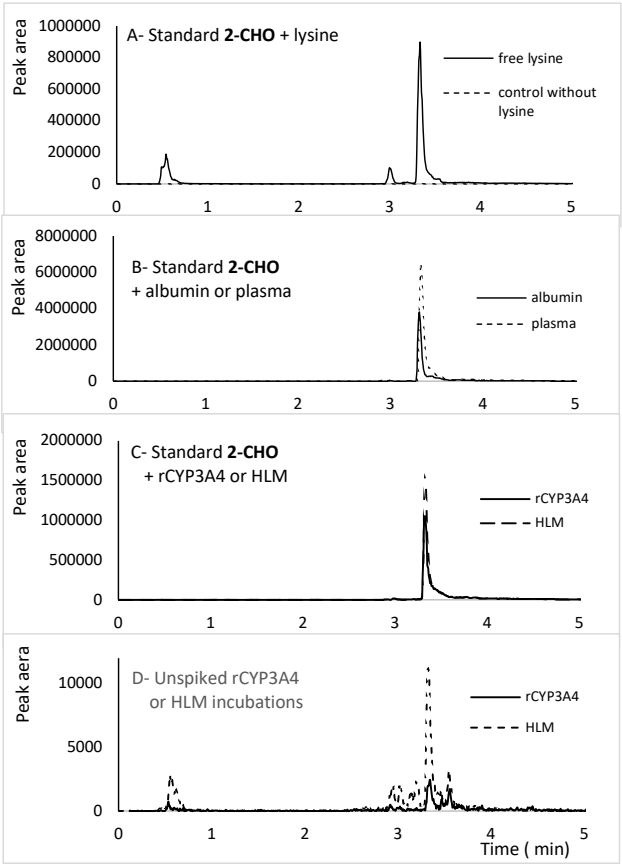
Peak area
1000000
800000
600000
400000
200000
0
A- Standard 2-CHO + lysine
free lysine
control without lysine
0 1 2 3 4 5
Peak area
8000000
6000000
4000000
2000000
0
B- Standard 2-CHO
+ albumin or plasma
albumin
plasma
0 1 2 3 4 5
Peak area
2000000
1500000
1000000
500000
0
C- Standard 2-CHO
+ rCYP3A4 or HLM
rCYP3A4
HLM
0 1 2 3 4 5
Peak aera
10000
5000
0
D- Unspiked rCYP3A4
or HLM incubations
rCYP3A4
HLM
0 1 2 3 4 5
Time (min)

Figure 6

559 **Supporting information:**

560 **Figure S-1**: Typical chromatograms of pazopanib aldehyde **1a-CHO** in patient plasma.

561 **Figure S-2**: Typical chromatograms of sunitinib aldehyde **2-CHO** in patient plasma.

562 **Figure S-3**: Molecular docking of pazopanib and sunitinib into CYP3A4 catalytic cavity.
563
564 **Figure S-4**: Molecular docking of pazopanib showing the orientation of C19 near the heme.

565 **Figure S-5**: Lysine residues in CYP3A4 protein framework.
566

567

568

569

5. REFERENCES

570 (1) Wu, P.; Nielsen, T. E.; Clausen, M. H. FDA-Approved Small-Molecule Kinase
571 Inhibitors. *Trends Pharmacol. Sci.* **2015**, *36* (7), 422–439.
572 https://doi.org/10.1016/j.tips.2015.04.005.
573 (2) Filppula, A. M.; Mustonen, T. M.; Backman, J. T. In Vitro Screening of Six
574 Protein Kinase Inhibitors for Time-Dependent Inhibition of CYP2C8 and
575 CYP3A4: Possible Implications with Regard to Drug-Drug Interactions.
576 *Basic Clin. Pharmacol. Toxicol.* **2018**.
577 https://doi.org/10.1111/bcpt.13088.
578 (3) Filppula, A. M.; Neuvonen, P. J.; Backman, J. T. In Vitro Assessment of
579 Time-Dependent Inhibitory Effects on CYP2C8 and CYP3A Activity by
580 Fourteen Protein Kinase Inhibitors. *Drug Metab. Dispos.* **2014**, *42* (7),
581 1202–1209. https://doi.org/10.1124/dmd.114.057695.
582 (4) Kenny, J. R.; Mukadam, S.; Zhang, C.; Tay, S.; Collins, C.; Galetin, A.;
583 Khojasteh, S. C. Drug-Drug Interaction Potential of Marketed Oncology
584 Drugs: In Vitro Assessment of Time-Dependent Cytochrome P450
585 Inhibition, Reactive Metabolite Formation and Drug-Drug Interaction
586 Prediction. *Pharm. Res.* **2012**, *29* (7), 1960–1976.
587 https://doi.org/10.1007/s11095-012-0724-6.
588 (5) Wang, Y.; Wang, M.; Qi, H.; Pan, P.; Hou, T.; Li, J.; He, G.; Zhang, H.
589 Pathway-Dependent Inhibition of Paclitaxel Hydroxylation by Kinase
590 Inhibitors and Assessment of Drug-Drug Interaction Potentials. *Drug*
591 *Metab. Dispos.* **2014**, *42* (4), 782–795.
592 https://doi.org/10.1124/dmd.113.053793.
593 (6) Zhang, J.; Ren, L.; Yang, X.; White, M.; Greenhaw, J.; Harris, T.; Wu, Q.;
594 Bryant, M.; Papoian, T.; Mattes, W.; et al. Cytotoxicity of 34 FDA
595 Approved Small-Molecule Kinase Inhibitors in Primary Rat and Human
596 Hepatocytes. *Toxicol. Lett.* **2018**, *291*, 138–148.
597 https://doi.org/10.1016/j.toxlet.2018.04.010.

(7) Jackson, K. D.; Durandis, R.; Vergne, M. J. Role of Cytochrome P450 Enzymes in the Metabolic Activation of Tyrosine Kinase Inhibitors. *Int J Mol Sci* **2018**, *19* (8). https://doi.org/10.3390/ijms19082367.
(8) Shah, R. R.; Morganroth, J.; Shah, D. R. Hepatotoxicity of Tyrosine Kinase Inhibitors: Clinical and Regulatory Perspectives. *Drug Saf* **2013**, *36* (7), 491–503. https://doi.org/10.1007/s40264-013-0048-4.
(9) Stepan, A. F.; Walker, D. P.; Bauman, J.; Price, D. A.; Baillie, T. A.; Kalgutkar, A. S.; Aleo, M. D. Structural Alert/Reactive Metabolite Concept as Applied in Medicinal Chemistry to Mitigate the Risk of Idiosyncratic Drug Toxicity: A Perspective Based on the Critical Examination of Trends in the Top 200 Drugs Marketed in the United States. *Chem. Res. Toxicol.* **2011**, *24* (9), 1345–1410. https://doi.org/10.1021/tx200168d.
(10) Orr, S. T. M.; Ripp, S. L.; Ballard, T. E.; Henderson, J. L.; Scott, D. O.; Obach, R. S.; Sun, H.; Kalgutkar, A. S. Mechanism-Based Inactivation (MBI) of Cytochrome P450 Enzymes: Structure-Activity Relationships and Discovery Strategies to Mitigate Drug-Drug Interaction Risks. *J. Med. Chem.* **2012**, *55* (11), 4896–4933. https://doi.org/10.1021/jm300065h.
(11) Park, B. K.; Boobis, A.; Clarke, S.; Goldring, C. E. P.; Jones, D.; Kenna, J. G.; Lambert, C.; Laverty, H. G.; Naisbitt, D. J.; Nelson, S.; et al. Managing the Challenge of Chemically Reactive Metabolites in Drug Development. *Nat Rev Drug Discov* **2011**, *10* (4), 292–306. https://doi.org/10.1038/nrd3408.
(12) Kalgutkar, A. S.; Dalvie, D. Predicting Toxicities of Reactive Metabolite-Positive Drug Candidates. *Annu. Rev. Pharmacol. Toxicol.* **2015**, *55*, 35–54. https://doi.org/10.1146/annurev-pharmtox-010814-124720.
(13) Silverman, R. B. Mechanism-Based Enzyme Inactivators. *Meth. Enzymol.* **1995**, *249*, 240–283.
(14) Orr, S. T. M.; Ripp, S. L.; Ballard, T. E.; Henderson, J. L.; Scott, D. O.; Obach, R. S.; Sun, H.; Kalgutkar, A. S. Mechanism-Based Inactivation (MBI) of Cytochrome P450 Enzymes: Structure-Activity Relationships and Discovery Strategies to Mitigate Drug-Drug Interaction Risks. *J. Med. Chem.* **2012**, *55* (11), 4896–4933. https://doi.org/10.1021/jm300065h.
(15) Sevrioukova, I. F.; Poulos, T. L. Current Approaches for Investigating and Predicting Cytochrome P450 3A4-Ligand Interactions. *Adv. Exp. Med. Biol.* **2015**, *851*, 83–105. https://doi.org/10.1007/978-3-319-16009-2_3.
(16) Fontana, E.; Dansette, P. M.; Poli, S. M. Cytochrome P450 Enzymes Mechanism Based Inhibitors: Common Sub-Structures and Reactivity. *Curr. Drug Metab.* **2005**, *6* (5), 413–454.
(17) Yu, H.; Balani, S. K.; Chen, W.; Cui, D.; He, L.; Humphreys, W. G.; Mao, J.; Lai, W. G.; Lee, A. J.; Lim, H.-K.; et al. Contribution of Metabolites to P450

Inhibition-Based Drug-Drug Interactions: Scholarship from the Drug Metabolism Leadership Group of the Innovation and Quality Consortium Metabolite Group. *Drug Metab. Dispos.* **2015**, *43* (4), 620–630. https://doi.org/10.1124/dmd.114.059345.

(18) Amaya, G. M.; Durandis, R.; Bourgeois, D. S.; Perkins, J. A.; Abouda, A. A.; Wines, K. J.; Mohamud, M.; Starks, S. A.; Daniels, R. N.; Jackson, K. D. Cytochromes P450 1A2 and 3A4 Catalyze the Metabolic Activation of Sunitinib. *Chem. Res. Toxicol.* **2018**, *31* (7), 570–584. https://doi.org/10.1021/acs.chemrestox.8b00005.

(19) Hardy, K. D.; Wahlin, M. D.; Papageorgiou, I.; Unadkat, J. D.; Rettie, A. E.; Nelson, S. D. Studies on the Role of Metabolic Activation in Tyrosine Kinase Inhibitor-Dependent Hepatotoxicity: Induction of CYP3A4 Enhances the Cytotoxicity of Lapatinib in HepaRG Cells. *Drug Metab. Dispos.* **2014**, *42* (1), 162–171. https://doi.org/10.1124/dmd.113.054817.

(20) Paech, F.; Bouitbir, J.; Krähenbühl, S. Hepatocellular Toxicity Associated with Tyrosine Kinase Inhibitors: Mitochondrial Damage and Inhibition of Glycolysis. *Front Pharmacol* **2017**, *8*, 367. https://doi.org/10.3389/fphar.2017.00367.

(21) Eno, M. R.; El-Gendy, B. E.-D. M.; Cameron, M. D. P450 3A-Catalyzed O-Dealkylation of Lapatinib Induces Mitochondrial Stress and Activates Nrf2. *Chem. Res. Toxicol.* **2016**, *29* (5), 784–796. https://doi.org/10.1021/acs.chemrestox.5b00524.

(22) Xie, C.; Zhou, J.; Guo, Z.; Diao, X.; Gao, Z.; Zhong, D.; Jiang, H.; Zhang, L.; Chen, X. Metabolism and Bioactivation of Famitinib, a Novel Inhibitor of Receptor Tyrosine Kinase, in Cancer Patients. *Br. J. Pharmacol.* **2013**, *168* (7), 1687–1706. https://doi.org/10.1111/bph.12047.

(23) Petrucci D, Hu C, French K, Webster L, Skordos K, Brown R, Jordan H, Cariello N, Miller R, Frazier K. Preclinical Investigations into Potential Mechanisms of Pazopanib-Induced Hepatotoxicity in Patients. Abstract 2262, p.492. 51st Annual Meeting and ToxExpo. Https://Www.Toxicology.Org/Pubs/Docs/Tox/2012Tox.Pdf. Accessed November 15, 2018. **2012**, *126* (1), 636.

(24) Paludetto, M.-N.; Bijani, C.; Puisset, F.; Bernardes-Génisson, V.; Arellano, C.; Robert, A. Metalloporphyrin-Catalyzed Oxidation of Sunitinib and Pazopanib, Two Anticancer Tyrosine Kinase Inhibitors: Evidence for New Potentially Toxic Metabolites. *J. Med. Chem.* **2018**, *61* (17), 7849–7860. https://doi.org/10.1021/acs.jmedchem.8b00812.

(25) Wang, Y.-K.; Yang, X.-N.; Liang, W.-Q.; Xiao, Y.; Zhao, Q.; Xiao, X.-R.; Gonzalez, F. J.; Li, F. A Metabolomic Perspective of Pazopanib-Induced Acute Hepatotoxicity in Mice. *Xenobiotica* **2018**, 1–16. https://doi.org/10.1080/00498254.2018.1489167.

(26) Castellino, S.; O'Mara, M.; Koch, K.; Borts, D. J.; Bowers, G. D.; MacLauchlin, C. Human Metabolism of Lapatinib, a Dual Kinase Inhibitor: Implications for Hepatotoxicity. *Drug Metab. Dispos.* **2012**, *40* (1), 139–150. https://doi.org/10.1124/dmd.111.040949.
(27) Liu, X.; Lu, Y.; Guan, X.; Dong, B.; Chavan, H.; Wang, J.; Zhang, Y.; Krishnamurthy, P.; Li, F. Metabolomics Reveals the Formation of Aldehydes and Iminium in Gefitinib Metabolism. *Biochem. Pharmacol.* **2015**, *97* (1), 111–121. https://doi.org/10.1016/j.bcp.2015.07.010.
(28) Kalgutkar, A. S. Liabilities Associated with the Formation of "Hard" Electrophiles in Reactive Metabolite Trapping Screens. *Chem. Res. Toxicol.* **2017**, *30* (1), 220–238. https://doi.org/10.1021/acs.chemrestox.6b00332.
(29) O'Brien, P. J.; Siraki, A. G.; Shangari, N. Aldehyde Sources, Metabolism, Molecular Toxicity Mechanisms, and Possible Effects on Human Health. *Crit. Rev. Toxicol.* **2005**, *35* (7), 609–662.
(30) Paludetto, M.-N.; Puisset, F.; Chatelut, E.; Arellano, C. Identifying the Reactive Metabolites of Tyrosine Kinase Inhibitors in a Comprehensive Approach: Implications for Drug-Drug Interactions and Hepatotoxicity. *Med Res Rev* **2019**. https://doi.org/10.1002/med.21577.
(31) Samuels, E. R.; Sevrioukova, I. Inhibition of Human CYP3A4 by Rationally Designed Ritonavir-Like Compounds: Impact and Interplay of the Side Group Functionalities. *Mol. Pharm.* **2018**, *15* (1), 279–288. https://doi.org/10.1021/acs.molpharmaceut.7b00957.
(32) Yano, J. K.; Wester, M. R.; Schoch, G. A.; Griffin, K. J.; Stout, C. D.; Johnson, E. F. The Structure of Human Microsomal Cytochrome P450 3A4 Determined by X-Ray Crystallography to 2.05-A Resolution. *J. Biol. Chem.* **2004**, *279* (37), 38091–38094. https://doi.org/10.1074/jbc.C400293200.
(33) Davis, I. W.; Murray, L. W.; Richardson, J. S.; Richardson, D. C. MOLPROBITY: Structure Validation and All-Atom Contact Analysis for Nucleic Acids and Their Complexes. *Nucleic Acids Res.* **2004**, *32* (Web Server issue), W615-619. https://doi.org/10.1093/nar/gkh398.
(34) Stewart, J. J. P. Optimization of Parameters for Semiempirical Methods VI: More Modifications to the NDDO Approximations and Re-Optimization of Parameters. *J Mol Model* **2013**, *19* (1), 1–32. https://doi.org/10.1007/s00894-012-1667-x.
(35) Trott, O.; Olson, A. J. AutoDock Vina: Improving the Speed and Accuracy of Docking with a New Scoring Function, Efficient Optimization, and Multithreading. *J Comput Chem* **2010**, *31* (2), 455–461. https://doi.org/10.1002/jcc.21334.
(36) Morris, G. M.; Huey, R.; Lindstrom, W.; Sanner, M. F.; Belew, R. K.; Goodsell, D. S.; Olson, A. J. AutoDock4 and AutoDockTools4: Automated Docking

with Selective Receptor Flexibility. *J Comput Chem* **2009**, *30* (16), 2785–2791. https://doi.org/10.1002/jcc.21256.
(37) Paludetto, M.-N.; Puisset, F.; Le Louedec, F.; Allal, B.; Lafont, T.; Chatelut, E.; Arellano, C. Simultaneous Monitoring of Pazopanib and Its Metabolites by UPLC-MS/MS. *J Pharm Biomed Anal* **2018**, *154*, 373–383. https://doi.org/10.1016/j.jpba.2018.03.013.
(38) Deng, Y.; Sychterz, C.; Suttle, A. B.; Dar, M. M.; Bershas, D.; Negash, K.; Qian, Y.; Chen, E. P.; Gorycki, P. D.; Ho, M. Y. K. Bioavailability, Metabolism and Disposition of Oral Pazopanib in Patients with Advanced Cancer. *Xenobiotica* **2013**, *43* (5), 443–453. https://doi.org/10.3109/00498254.2012.734642.
(39) Food and Drug Administration. Product Review. Https://Www.Accessdata.Fda.Gov/Drugsatfda_docs/Nda/2006/021938_S000_Sutent_PharmR.Pdf. Accessed January 10, 2019.
(40) Speed, B.; Bu, H.-Z.; Pool, W. F.; Peng, G. W.; Wu, E. Y.; Patyna, S.; Bello, C.; Kang, P. Pharmacokinetics, Distribution, and Metabolism of [14C]Sunitinib in Rats, Monkeys, and Humans. *Drug Metab. Dispos.* **2012**, *40* (3), 539–555. https://doi.org/10.1124/dmd.111.042853.
(41) Belloc, C.; Gauffre, A.; André, C.; Beaune, P. H. Epitope Mapping of Human CYP1A2 in Dihydralazine-Induced Autoimmune Hepatitis. *Pharmacogenetics* **1997**, *7* (3), 181–186.
(42) Bourdi, M.; Gautier, J. C.; Mircheva, J.; Larrey, D.; Guillouzo, A.; Andre, C.; Belloc, C.; Beaune, P. H. Anti-Liver Microsomes Autoantibodies and Dihydralazine-Induced Hepatitis: Specificity of Autoantibodies and Inductive Capacity of the Drug. *Mol. Pharmacol.* **1992**, *42* (2), 280–285.
(43) Grilo, N. M.; Charneira, C.; Pereira, S. A.; Monteiro, E. C.; Marques, M. M.; Antunes, A. M. M. Bioactivation to an Aldehyde Metabolite--Possible Role in the Onset of Toxicity Induced by the Anti-HIV Drug Abacavir. *Toxicol. Lett.* **2014**, *224* (3), 416–423. https://doi.org/10.1016/j.toxlet.2013.10.036.
(44) Charneira, C.; Godinho, A. L. A.; Oliveira, M. C.; Pereira, S. A.; Monteiro, E. C.; Marques, M. M.; Antunes, A. M. M. Reactive Aldehyde Metabolites from the Anti-HIV Drug Abacavir: Amino Acid Adducts as Possible Factors in Abacavir Toxicity. *Chem. Res. Toxicol.* **2011**, *24* (12), 2129–2141. https://doi.org/10.1021/tx200337b.
(45) Meng, X.; Maggs, J. L.; Usui, T.; Whitaker, P.; French, N. S.; Naisbitt, D. J.; Park, B. K. Auto-Oxidation of Isoniazid Leads to Isonicotinic-Lysine Adducts on Human Serum Albumin. *Chem. Res. Toxicol.* **2015**, *28* (1), 51–58. https://doi.org/10.1021/tx500285k.
(46) Meng, X.; Howarth, A.; Earnshaw, C. J.; Jenkins, R. E.; French, N. S.; Back, D. J.; Naisbitt, D. J.; Park, B. K. Detection of Drug Bioactivation in Vivo: Mechanism of Nevirapine-Albumin Conjugate Formation in Patients. *Chem.*

Res. Toxicol. **2013**, *26* (4), 575–583. https://doi.org/10.1021/tx4000107.
(47) Sabbioni, G.; Turesky, R. J. Biomonitoring Human Albumin Adducts: The Past, the Present, and the Future. *Chem. Res. Toxicol.* **2017**, *30* (1), 332–366. https://doi.org/10.1021/acs.chemrestox.6b00366.
(48) Cai, J.; Hill, B. G.; Bhatnagar, A.; Pierce, W. M.; Prough, R. A. Bioactivation and Protein Modification Reactions of Unsaturated Aldehydes. In *Advances in Bioactivation Research*; Elfarra, A., Ed.; Biotechnology: Pharmaceutical Aspects; Springer New York: New York, NY, 2008; pp 1–21. https://doi.org/10.1007/978-0-387-77300-1_9.
(49) Trézl, L.; Hullán, L.; Jászay, Z. M.; Szarvas, T.; Petneházy, I.; Szende, B.; Bocsi, J.; Takáts, Z.; Vékey, K.; Töke, L. Antagonistic Reactions of Arginine and Lysine against Formaldehyde and Their Relation to Cell Proliferation, Apoptosis, Folate Cycle and Photosynthesis. *Mol. Cell. Biochem.* **2003**, *244* (1–2), 167–176.
(50) Metz, B.; Kersten, G. F. A.; Hoogerhout, P.; Brugghe, H. F.; Timmermans, H. A. M.; de Jong, A.; Meiring, H.; ten Hove, J.; Hennink, W. E.; Crommelin, D. J. A.; et al. Identification of Formaldehyde-Induced Modifications in Proteins: Reactions with Model Peptides. *J. Biol. Chem.* **2004**, *279* (8), 6235–6243. https://doi.org/10.1074/jbc.M310752200.
(51) Mingard, C.; Paech, F.; Bouitbir, J.; Krähenbühl, S. Mechanisms of Toxicity Associated with Six Tyrosine Kinase Inhibitors in Human Hepatocyte Cell Lines. *J Appl Toxicol* **2018**, *38* (3), 418–431. https://doi.org/10.1002/jat.3551.
(52) Zhang, J.; Salminen, A.; Yang, X.; Luo, Y.; Wu, Q.; White, M.; Greenhaw, J.; Ren, L.; Bryant, M.; Salminen, W.; et al. Effects of 31 FDA Approved Small-Molecule Kinase Inhibitors on Isolated Rat Liver Mitochondria. *Arch. Toxicol.* **2017**, *91* (8), 2921–2938. https://doi.org/10.1007/s00204-016-1918-1.
(53) Qosa, H.; Avaritt, B. R.; Hartman, N. R.; Volpe, D. A. In Vitro UGT1A1 Inhibition by Tyrosine Kinase Inhibitors and Association with Drug-Induced Hyperbilirubinemia. *Cancer Chemother. Pharmacol.* **2018**, *82* (5), 795–802. https://doi.org/10.1007/s00280-018-3665-x.
(54) Morgan, R. E.; van Staden, C. J.; Chen, Y.; Kalyanaraman, N.; Kalanzi, J.; Dunn, R. T.; Afshari, C. A.; Hamadeh, H. K. A Multifactorial Approach to Hepatobiliary Transporter Assessment Enables Improved Therapeutic Compound Development. *Toxicol. Sci.* **2013**, *136* (1), 216–241. https://doi.org/10.1093/toxsci/kft176.
(55) Xu, C.-F.; Johnson, T.; Wang, X.; Carpenter, C.; Graves, A. P.; Warren, L.; Xue, Z.; King, K. S.; Fraser, D. J.; Stinnett, S.; et al. HLA-B*57:01 Confers Susceptibility to Pazopanib-Associated Liver Injury in Patients with Cancer. *Clin. Cancer Res.* **2016**, *22* (6), 1371–1377. https://doi.org/10.1158/1078-0432.CCR-15-2044.

(56) Xu, C.-F.; Reck, B. H.; Goodman, V. L.; Xue, Z.; Huang, L.; Barnes, M. R.; Koshy, B.; Spraggs, C. F.; Mooser, V. E.; Cardon, L. R.; et al. Association of the Hemochromatosis Gene with Pazopanib-Induced Transaminase Elevation in Renal Cell Carcinoma. *J. Hepatol.* **2011**, *54* (6), 1237–1243. https://doi.org/10.1016/j.jhep.2010.09.028.

Mis en forme : Anglais (E.U.)

CONFLICT OF INTEREST

The authors declare that they have no conflict of interest.

ACKNOWLEDGMENTS

The authors thank Dr. Ben Allal for handling sunitinib plasma samples, and are grateful to Dr. Catherine Claparols, head of the mass spectrometry department of the Institut de Chimie de Toulouse (ICT, Toulouse, France) for her help with the analyses performed on the QTRAP 4500 mass spectrometer. The authors also wish to thank Gail Taillefer, PhD (Emeritus professor of English) for her help with English language editing. This research received no specific grant from any funding agency in the public, commercial, or not-for-profit sectors.